

Subspace Fusion Sensing for Cooperative ISAC

Yining Xu, Cunhua Pan, *Senior Member, IEEE*, Jun Tang, Hong Ren, and Jiangzhou Wang, *Fellow, IEEE*

Abstract—This paper proposes a subspace fusion sensing algorithm for cooperative integrated sensing and communication. First, we stack the received signals from access points (APs) into a third-order tensor and construct the equivalent virtual antenna (EVA) array via tensor unfolding. Then, a data association-free subspace-based fusion sensing algorithm is developed utilizing the EVA arrays from distributed APs. A derivation of Cramér-Rao lower bound (CRLB) is also presented. Finally, simulation results validate the effectiveness of the proposed algorithm compared to traditional techniques.

Index Terms—Cooperative integrated communication and sensing, tensor, data fusion.

I. INTRODUCTION

Integrated sensing and communication (ISAC) has been envisioned as a pivotal technology for the sixth-generation (6G) mobile networks, supporting emerging applications such as the low-altitude economy [1] and autonomous driving [2]. However, conventional ISAC systems typically operate in a single-node configuration, where an individual base station (BS) performs sensing tasks independently via signal processing techniques such as tensor decomposition [3] and compressive sensing [4]. This configuration faces inherent physical limitations. In particular, the severe round-trip path loss and the limited power of BSs significantly degrade sensing performance for distant targets, which is exacerbated when line-of-sight (LoS) paths are obstructed.

To mitigate these issues, cooperative ISAC has emerged as a promising paradigm, leveraging existing communication networks for multi-node cooperative sensing. Recently, several cooperative sensing schemes have been proposed. Tang et al. proposed a multi-target sensing algorithm based on tensor decomposition [5]. Zhang et al. developed a single-antenna sensing scheme utilizing maximum likelihood estimation (MLE) [6]. Liu et al. utilized multipath components to establish virtual BSs to sense a single target [7]. Liu et al. proposed a Bayesian probability fusion approach for cooperative ISAC [8]. However, most existing works rely on two-stage framework including complex data association, which may not fully exploit the cooperative sensing gain. In this paper, different from the aforementioned works, we propose a novel cooperative sensing algorithm based on subspace fusion. The main contributions are summarized as follows:

- We construct equivalent virtual antenna (EVA) arrays via tensor unfolding to synthesize a larger sensing aperture.
- We propose an association-free subspace fusion algorithm for high-precision sensing.

Yining Xu, Cunhua Pan, Jun Tang, Hong Ren and Jiangzhou Wang are with National Mobile Communications Research Laboratory, Southeast University, Nanjing 210096, China (e-mail: yining.xu, cpan, 220241016, hren and j.z.wang@seu.edu.cn). *Corresponding authors: Cunhua pan*

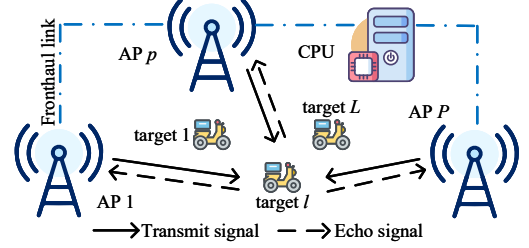


Fig. 1: cooperative ISAC system.

- We derive the Cramér-Rao lower bound (CRLB) and verify its superiority over traditional techniques.

II. SYSTEM MODEL

The cooperative ISAC system is illustrated in Fig. 1. Consider a cellular network comprising P access points (AP) to sense L targets. Each AP utilizes uniform linear arrays (ULA) with M antenna elements and operates in the monostatic mode. The APs broadcast 5G New Radio (5G NR) orthogonal frequency-division multiplexing (OFDM) signals across P distinct frequency bands and the central control unit (CPU) aggregates the sensing data for joint estimation. The transmitted signal of the p th AP is denoted as

$$s_p(t) = \sum_{k=1}^K \sum_{n=1}^N s_{p,k,n} e^{j2\pi k \Delta f t} \cdot r(t - nT_s), \quad (1)$$

where K and N are respectively the number of subcarriers and OFDM symbols, $s_{p,k,n}$ is the modulated symbols allocated in the k th subcarrier, n th OFDM symbol at the p th AP, T_s is the OFDM symbol period (including the cyclic prefix), $r(t)$ is the pulse-shaping filter function and Δf is the subcarrier spacing (SCS). Without loss of generality, we assume that $|s_{p,k,n}|^2 = 1, \forall p, k, n$. The frequency domain signal vector is given by

$$\mathbf{y}_{p,k,n} = \mathbf{H}_{p,k,n} \mathbf{f}_p s_{p,k,n} + \mathbf{n}_{p,k,n}, \quad (2)$$

where $\mathbf{f}_p \in \mathbb{C}^{M \times 1}$ denotes the beamforming vector at the p th AP, $\mathbf{H}_{p,k,n} \in \mathbb{C}^{M \times M}$ denotes the discrete frequency-domain monostatic channel at the p th AP and $\mathbf{n}_{p,k,n} \in \mathbb{C}^{M \times 1}$ denotes the additive white Gaussian noise (AWGN) vector. To eliminate the sensing symbols, the received signal is divided by the transmitted symbols, i.e.,

$$\hat{\mathbf{y}}_{p,k,n} = \mathbf{y}_{p,k,n} / s_{p,k,n} = \mathbf{H}_{p,k,n} \mathbf{f}_p + \hat{\mathbf{n}}_{p,k,n}, \quad (3)$$

where $\hat{\mathbf{n}}_{p,k,n}$ denotes the equivalent noise vector.

Then, the time and delay domain sensing channel is modeled as

$$\mathbf{H}_p(t, \tau) = \sum_{l=1}^L \alpha_{p,l} \delta(\tau - \tau_{p,l}) \mathbf{a}_p(\theta_{p,l}) \cdot \mathbf{a}_p^H(\theta_{p,l}) e^{j2\pi f_p^d t}, \quad (4)$$

where $\alpha_{p,l}$, $\tau_{p,l} = 2d_{p,l}/c$ and $f_{p,l}^d = 2v_{p,l}/\lambda$ are respectively the complex channel gains, delay and Doppler shift. The symbols $d_{p,l}$, $v_{p,l}$ are respectively the range and radial velocity. The symbols c and λ are respectively the speed of light and wavelength. The symbol $\theta_{p,l}$ is the angle of arrive (AoA). For brevity, we define the virtual angle as $\psi_{p,l} \triangleq \cos(\theta_{p,l})$. Thus, the steering vector at the p th AP for the l th target is rewritten as $\mathbf{a}_p(\psi_{p,l}) = [1, \dots, e^{j2\pi(M-1)\frac{d}{\lambda}\psi_{p,l}}]^T$. Then, following the Fourier transform (FT) over the delay and sampling at the n th OFDM symbol, the discrete frequency domain channel is given by

$$\mathbf{H}_{p,k,n} = \sum_{l=1}^L \alpha_{p,l} \mathbf{a}_p(\psi_{p,l}) \mathbf{a}_p^H(\psi_{p,l}) e^{-j2\pi k \Delta f \tau_{p,l}} e^{j2\pi f_{p,l}^d n T_s}. \quad (5)$$

III. SUBSPACE FUSION SENSING ALGORITHM

By substituting (5) into (2), the received signal at the p th AP is written as a third-order tensor $\mathcal{Y}_p \in \mathbb{C}^{M \times N \times K}$, i.e.,

$$\mathcal{Y}_p = \sum_{l=1}^L \beta_{p,l} \mathbf{a}_p(\psi_{p,l}) \circ \mathbf{o}_p(f_{p,l}^d) \circ \mathbf{g}_p(\tau_{p,l}) + \mathcal{N}_p, \quad (6)$$

where $\mathcal{N}_p \in \mathbb{C}^{M \times N \times K}$ is the equivalent noise tensor and $\beta_{p,l} = \alpha_{p,l} \mathbf{a}_p^H(\psi_{p,l}) \mathbf{f}_p$, $\mathbf{o}_p(f_{p,l}^d) = [e^{j2\pi T_s f_{p,l}^d}, \dots, e^{j2\pi N T_s f_{p,l}^d}]^T \in \mathbb{C}^{N \times 1}$, $\mathbf{g}_p(\tau_{p,l}) = [e^{-j2\pi \Delta f \tau_{p,l}}, \dots, e^{-j2\pi K \Delta f \tau_{p,l}}]^T \in \mathbb{C}^{K \times 1}$ and \circ denotes the vector outer product. The factor matrices of \mathcal{Y}_p are respectively denoted as $\mathbf{A}_p = [\mathbf{a}_p(\psi_{p,1}), \dots, \mathbf{a}_p(\psi_{p,L})] \in \mathbb{C}^{M \times L}$, $\mathbf{O}_p = [\mathbf{o}_p(f_{p,1}^d), \dots, \mathbf{o}_p(f_{p,L}^d)] \in \mathbb{C}^{N \times L}$ and $\mathbf{G}_p = [\mathbf{g}_p(\tau_{p,1}), \dots, \mathbf{g}_p(\tau_{p,L})] \in \mathbb{C}^{K \times L}$. For brevity, we omit the noise term in the subsequent derivations. By taking the n th slice of the tensor \mathcal{Y}_p , we obtain

$$\begin{aligned} \mathbf{Y}_{p,n} &= \sum_{l=1}^L \gamma_{p,n,l} \cdot \mathbf{a}_p(\psi_{p,l}) \mathbf{g}_p^T(\tau_{p,l}) \\ &= \mathbf{A}_p \mathbf{D}_{p,n} \mathbf{G}_p^T. \end{aligned} \quad (7)$$

where $\gamma_{p,n,l} = \beta_{p,l} e^{j2\pi f_{p,l}^d n T_s}$, $\mathbf{D}_{p,n} = \text{diag}(\mathbf{s}_{p,n})$ and $\mathbf{s}_{p,n} = [\gamma_{p,n,1}, \dots, \gamma_{p,n,L}]^T$. By performing the vec operator, we have

$$\begin{aligned} \mathbf{y}_{p,n} &= \text{vec}(\mathbf{Y}_{p,n}) = ((\mathbf{G}_p^T)^T \otimes \mathbf{A}_p) \text{vec}(\mathbf{D}_{p,n}) \\ &= (\mathbf{G}_p \odot \mathbf{A}_p) \mathbf{s}_{p,n} \triangleq \mathbf{\Pi}_p \mathbf{s}_{p,n}, \end{aligned} \quad (8)$$

where \otimes and \odot are respectively the Kronecker product and Khatri-Rao product. The unknown parameters in (8) can be expressed as $\boldsymbol{\xi} = [\text{Re}(\mathbf{s})^T, \text{Im}(\mathbf{s})^T, \mathbf{e}^T]^T$ where $\mathbf{s} = [\mathbf{s}_1^T, \dots, \mathbf{s}_P^T]^T$, $\mathbf{s}_p = [\mathbf{s}_{p,1}^T, \dots, \mathbf{s}_{p,N}^T]^T$, $\mathbf{e} = [\mathbf{p}_1^{t,T}, \dots, \mathbf{p}_L^{t,T}]^T$ and $\mathbf{p}_l^t = [x_l^t, y_l^t]^T$ is the position of the l th target. Therefore, the likelihood function for $\boldsymbol{\xi}$ is expressed as

$$f(\mathbf{y}|\boldsymbol{\xi}) = \frac{1}{(\pi\sigma_n^2)^{MKNP}} e^{-\frac{1}{\sigma_n^2} \sum_{p,n} \|\mathbf{y}_{p,n} - \mathbf{\Pi}_p \mathbf{s}_{p,n}\|^2}, \quad (9)$$

where $\mathbf{y} = [\mathbf{y}_1^T, \dots, \mathbf{y}_P^T]^T$, $\mathbf{y}_p = \text{vec}(\mathcal{Y}_p)$, σ_n^2 is the variance of the AWGN and $\|\cdot\|$ denotes the L2-norm. According to (9), the log-likelihood function can be expressed as

$$f_{ln}(\mathbf{y}|\boldsymbol{\xi}) = -MKNP \ln \pi \sigma_n^2 - \frac{1}{\sigma_n^2} \sum_{p,n} \|\mathbf{y}_{p,n} - \mathbf{\Pi}_p \mathbf{s}_{p,n}\|^2.$$

We define $S_{p,n}(\boldsymbol{\xi}) = \sum_{p,n} \|\mathbf{y}_{p,n} - \mathbf{\Pi}_p \mathbf{s}_{p,n}\|^2$. Differentiating $f_{ln}(\mathbf{y}|\boldsymbol{\xi})$ with respect to σ_n^2 and letting it equal to 0, we have

$$\frac{\partial f_{ln}}{\partial \sigma_n^2} = -\frac{MKNP}{\sigma_n^2} + \frac{S_{p,n}(\boldsymbol{\xi})}{(\sigma_n^2)^2} = 0. \quad (10)$$

Thus, the noise power can be estimated as $\hat{\sigma}_n^2 = \frac{1}{MKNP} S_{p,n}(\boldsymbol{\xi})$. By substituting $\hat{\sigma}_n^2$ into (10), we have

$$f_{ln}(\mathbf{y}|\boldsymbol{\xi}) = -MKNP \ln \hat{\sigma}_n^2 - \frac{S_{p,n}(\boldsymbol{\xi})}{\hat{\sigma}_n^2} \propto -\ln(S_{p,n}(\boldsymbol{\xi})),$$

where \propto denotes proportionality. Thus, we can obtain the optimal $\boldsymbol{\xi}$ by minimizing the following cost function, i.e.,

$$\hat{\boldsymbol{\xi}} = \arg \min_{\boldsymbol{\xi}} \ln(S_{p,n}(\boldsymbol{\xi})). \quad (11)$$

Problem (11) presents a high-dimensional, nonlinear optimization challenge characterized by a complex cost function. Consequently, deriving a closed-form analytical expression for $\hat{\boldsymbol{\xi}}$ is mathematically intractable. Although exhaustive grid search methods could theoretically locate the global optimum, the associated computational complexity is prohibitively high, rendering such an approach impractical for practical applications. Therefore, we simplify this problem from a subspace perspective to reduce the dimension of searching. A concept named EVA array is proposed in Fig. 2a. Specifically, we can fully exploit the degrees of freedom in both the spatial and frequency domains to achieve enhanced sensing performance by treating the signals received across M physical antennas and K subcarriers as observations from a virtual antenna array with MK equivalent elements. To achieve this idea, we first perform the mode-2 unfolding of \mathcal{Y}_p , given by

$$\mathbf{Y}_{(2)} = (\mathbf{G}_p \odot \mathbf{A}_p) \mathbf{O}_p^T. \quad (12)$$

The mode-2 unfolding operation in (12) stacks the spatial dimension and the frequency dimension. Thus, each EVA corresponds to a specific combination of a physical antenna index and a subcarrier index in the EVA array. Then, the covariance matrix of (12) can be estimated as

$$\hat{\mathbf{R}}_p = \frac{1}{N} \mathbf{Y}_{(2)}^H \mathbf{Y}_{(2)} = \frac{1}{N} (\mathbf{G}_p \odot \mathbf{A}_p) \hat{\mathbf{R}}_{o,p} (\mathbf{G}_p \odot \mathbf{A}_p)^H, \quad (13)$$

where $\hat{\mathbf{R}}_{o,p} = \mathbf{O}_p^T \mathbf{O}_p^*$. By performing the eigenvalue decomposition (EVD) of $\hat{\mathbf{R}}_p$, we have

$$\hat{\mathbf{R}}_p = \sum_{i=0}^L \lambda_i \boldsymbol{\mu}_i \boldsymbol{\mu}_i^H + \sum_{i=L+1}^{MK-1} \lambda_i \boldsymbol{\mu}_i \boldsymbol{\mu}_i^H, \quad (14)$$

where λ_i and $\boldsymbol{\mu}_i$ are the i th eigenvalue and eigenvector of $\hat{\mathbf{R}}_p$, respectively. The eigenvalues are sorted in non-decreasing order. Thus, $\mathbf{U}_{p,a} = [\boldsymbol{\mu}_0, \dots, \boldsymbol{\mu}_L]$ forms the signal subspace and $\mathbf{U}_{p,w} = [\boldsymbol{\mu}_{L+1}, \dots, \boldsymbol{\mu}_{MK-1}]$ forms the noise subspace. By utilizing the EVA array, the dimension of the noise subspace $\mathbf{U}_{p,w}$ is expanded to $MK - L$. Based on the EVA array structure in (12), for any given candidate position \mathbf{p}^t , the steering vector of the EVA array is constructed as

$$\boldsymbol{\omega}(\mathbf{p}^t) = \mathbf{o}(\tau(\mathbf{p}^t)) \otimes \mathbf{a}(\psi(\mathbf{p}^t)), \quad (15)$$

where $\mathbf{o}(\tau(\mathbf{p}^t))$ and $\mathbf{a}(\psi(\mathbf{p}^t))$ are defined in (6), which captures the phase variation across subcarriers and antennas respectively. This construction maps the range and angle information of the target into a unified high-dimensional subspace, eliminating data association and enabling high-precision sensing via orthogonality. The candidate delay $\tau(\mathbf{p}^t)$ and angle $\psi(\mathbf{p}^t)$ are respectively expressed as

$$\tau(\mathbf{p}^t) = \frac{\|\mathbf{T}^{-1}(\kappa_p)\mathbf{p}^t - \mathbf{T}^{-1}(\kappa_p)\mathbf{p}_p^a\|}{2c}, \quad (16)$$

$$\begin{bmatrix} \psi(\mathbf{p}^t) \\ \sin(\psi^{-1}(\mathbf{p}^t)) \end{bmatrix} = \frac{\mathbf{T}^{-1}(\kappa_p)\mathbf{p}^t - \mathbf{T}^{-1}(\kappa_p)\mathbf{p}_p^a}{\|\mathbf{T}^{-1}(\kappa_p)\mathbf{p}^t - \mathbf{T}^{-1}(\kappa_p)\mathbf{p}_p^a\|}, \quad (17)$$

where $\psi^{-1} = \cos^{-1}(\psi(\mathbf{p}^t))$, $\mathbf{p}_p^a = [x_p^a, y_p^a]^T$ is the position of the p th AP, κ_p is the angle between the local and global coordinate systems at the p th AP, as shown in Fig. 2b and $\mathbf{T}(\kappa_p)$ is the transformation matrix from the local coordinate to the global coordinate at the p th AP, given by

$$\mathbf{T}(\kappa_p) = \begin{bmatrix} \cos(\kappa_p) & \sin(\kappa_p) \\ -\sin(\kappa_p) & \cos(\kappa_p) \end{bmatrix}. \quad (18)$$

Combining the observed data of APs, we define the cost function of subspace fusion sensing problem as

$$\Psi(\mathbf{p}^t) = \frac{1}{\sum_{p=1}^P \boldsymbol{\omega}^H(\mathbf{p}^t)\mathbf{U}_{p,w}\mathbf{U}_{p,w}^H\boldsymbol{\omega}(\mathbf{p}^t)}. \quad (19)$$

The subspace fusion sensing algorithm is shown in Algorithm 1. To find the L peaks of (19), we firstly construct a coarse grid set \mathbb{S}_{coarse} including $L_x \times L_y$ points. Then, we can obtain the coarse estimate of the target position by finding the L peaks of (19). Finally, a coarse estimate is used as the initial value and solve (11) with the Quasi-Newton method [9] to obtain the final estimate.

Complexity Analysis: The mode-2 tensor unfolding, covariance matrix estimation and EVD for P APs require a complexity of $\mathcal{O}(PNM^2K^2 + PM^3K^3)$. Evaluating the cost function over $L_x \times L_y$ grid points yields a complexity of $\mathcal{O}(PL_xL_yM^2K^2)$. The fine search utilizing the Quasi-Newton method for L targets incurs a complexity of $\mathcal{O}(PLIM^2K^2)$, where I is the number of iterations. It is worth noting that our proposed algorithm expands the array aperture by constructing the EVA to achieve higher sensing accuracy, this comes at the cost of increased computational complexity. Therefore, the algorithm is well-suited for resource-constrained scenarios with a limited number of antennas or subcarriers. Since communication-centric ISAC systems allocate only a small fraction of resources for sensing, the actual computational overhead remains manageable, rendering the proposed algorithm practical for future cooperative networks.

IV. CRAMÉR-RAO LOWER BOUND

For the l th target, define the unknown parameter vector as $\boldsymbol{\Xi}_l = [\tau_{1,l}, \dots, \tau_{P,l}, \psi_{p,1}^g, \dots, \psi_{P,l}^g]^T$. According to (6), the ISAC echo signal of the AP p sensing signal can be expressed as

$$y_{p,l} = \sum_{m,k,n} \beta_{p,l} e^{j2\pi f_{p,l}^d n T_s} e^{-j2\pi k \Delta f \tau_{p,l}} e^{j2\pi m \psi_{p,l}^g d/\lambda} + n_{p,l}, \quad (20)$$

Algorithm 1 Subspace Fusion Sensing Algorithm

Step 1: Subspace Estimation

- 1: **for** $p = 1$ to P **do**
- 2: Perform mode-2 unfolding of \mathcal{Y}_p via (12).
- 3: Estimate the covariance matrix $\hat{\mathbf{R}}_p$ via (13).
- 4: Perform EVD on $\hat{\mathbf{R}}_p$ to obtain the noise subspace $\mathbf{U}_{p,w}$ according to (14).

5: **end for**

Step 2: Coarse Search

- 6: Define a coarse grid set \mathbb{S}_{coarse} including $L_x \times L_y$ points.
- 7: **for** each grid point $\mathbf{p}^t \in \mathbb{S}_{coarse}$ **do**
- 8: Calculate $\boldsymbol{\omega}(\mathbf{p}^t)$ via (15), (16), (17) and (18).
- 9: Compute $\Psi(\mathbf{p}^t)$ via (19).

10: **end for**

11: Obtain the coarse estimate $\{\hat{\mathbf{p}}_l^{t,coarse} | l = 1, \dots, L\}$ by finding the L peaks of (19).

Step 3: Fine Search

- 12: **for** $l = 1$ to L **do**
- 13: Use the coarse estimate $\hat{\mathbf{p}}_l^{t,coarse}$ as the initial value.
- 14: Solve $\hat{\mathbf{p}}_l^t = \arg \max_{\mathbf{p}_l^t} \Psi(\mathbf{p}_l^t)$ with the Quasi-Newton method and obtain the final estimate $\hat{\mathbf{p}}_l^t$.
- 15: **end for**

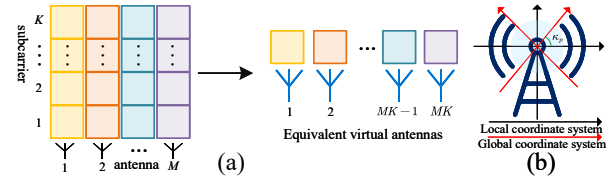


Fig. 2: Illustration of (a) EVA array construction and (b) local and global coordinate systems at the AP.

where $\psi_{p,l}^g$ is the virtual angle in the global coordinate. Based on (20), the probability density function (PDF) of $\boldsymbol{\Xi}_l$ is

$$q(\mathbf{u}; \boldsymbol{\Xi}_l) = \frac{1}{(2\pi\sigma_n^2)^{L/2}} e^{-\frac{1}{2\sigma_n^2} \sum_{l=1}^L |y_{p,l} - \sum_{m,k,n} s_{p,l,m,k,n}|^2}, \quad (21)$$

where $\mathbf{u} = [y_{p,1}, \dots, y_{p,L}]^T$ denotes a set of echo signals received by P APs and $s_{p,l,m,k,n} = \beta_{p,l} e^{j2\pi f_{p,l}^d n T_s} e^{-j2\pi k \Delta f \tau_{p,l}} e^{j2\pi m \psi_{p,l}^g d/\lambda}$. The log-likelihood function of $\boldsymbol{\Xi}_l$ is given by

$$q_{ln}(\mathbf{u}; \boldsymbol{\Xi}_l) = -\frac{P}{2} \ln(2\pi\sigma_n^2) - \frac{1}{2\sigma_n^2} \sum_{p=1}^P \left| y_p^l - \sum_{m,k,n} s_{p,l,m,k,n} \right|^2. \quad (22)$$

According to the definition of the Fisher information matrix (FIM), the entries of the matrix are determined by the Hessian of the log-likelihood function. By taking the second-order partial derivatives of (22) with respect to the parameter vector $\boldsymbol{\Xi}_l$ and computing the expectation, the (i, j) th element of the FIM is obtained as

$$\begin{aligned} [\mathbf{F}]_{i,j} &= \mathbb{E} \left(-\frac{\partial q_{ln}(\mathbf{u}; \boldsymbol{\Xi}_l)}{\partial [\boldsymbol{\Xi}_l]_i \partial [\boldsymbol{\Xi}_l]_j} \right) \\ &= \frac{2}{\sigma_n^2} \text{Re} \left\{ \left(\frac{\partial s_l(\boldsymbol{\Xi}_l)}{\partial [\boldsymbol{\Xi}_l]_i} \right)^H \left(\frac{\partial s_l(\boldsymbol{\Xi}_l)}{\partial [\boldsymbol{\Xi}_l]_j} \right) \right\}, \quad (23) \end{aligned}$$

where $\mathbf{s}_l = [s_{1,l}, \dots, s_{P,l}]^T$ and $s_{p,l} = \sum_{m,k,n} s_{p,l,m,k,n}$. We firstly calculate the partial derivatives of $s_{p,l}$ with respect to $\tau_{p,l}$ and $\psi_{p,l}^g$ as follows

$$\frac{\partial s_{p,l}}{\partial \tau_{p,l}} = \frac{\partial \sum_{m,k,n} \beta_{p,l} e^{j2\pi f_{p,l}^d n T_s} e^{-j2\pi k \Delta f \tau_{p,l}} e^{j2\pi m \psi_{p,l}^g d / \lambda}}{\partial \tau_{p,l}} = \sum_{m,k,n} -j2\pi n \Delta f s_{p,l,m,k,n}, \quad (24)$$

$$\frac{\partial s_{p,l}}{\partial \psi_{p,l}^g} = \frac{\partial \sum_{m,k,n} \beta_{p,l} e^{j2\pi f_{p,l}^d n T_s} e^{-j2\pi k \Delta f \tau_{p,l}} e^{j2\pi m \psi_{p,l}^g d / \lambda}}{\partial \psi_{p,l}^g} = \sum_{m,k,n} j2\pi m d s_{p,l,m,k,n} / \lambda. \quad (25)$$

According to the above derivations, the FIM consists of four block diagonal matrices, given by

$$\mathbf{F} = \begin{bmatrix} \mathbf{\Psi} & \mathbf{\Upsilon} \\ \mathbf{\Upsilon} & \mathbf{\Omega} \end{bmatrix}, \quad (26)$$

where $\mathbf{\Psi} \in \mathbb{C}^{P \times P}$, $\mathbf{\Omega} \in \mathbb{C}^{P \times P}$ and $\mathbf{\Upsilon} \in \mathbb{C}^{P \times P}$ are diagonal matrices. The diagonal elements of these matrices can be calculated as follows

$$\begin{aligned} \Psi_{p,p} &= \frac{2}{\sigma_n^2} \text{Re} \left\{ \left(\frac{\partial s_{p,l}}{\partial \tau_{p,l}} \right)^* \left(\frac{\partial s_{p,l}}{\partial \tau_{p,l}} \right) \right\} \\ &= \frac{2}{\sigma_n^2} \sum_{m,k,n} |\beta_{p,l}|^2 (2\pi n \Delta f)^2 \\ &= \frac{4\pi^2 |\beta_{p,l}|^2 \Delta f^2 M K N (N+1) (2N+1)}{3\sigma_n^2}, \end{aligned} \quad (27)$$

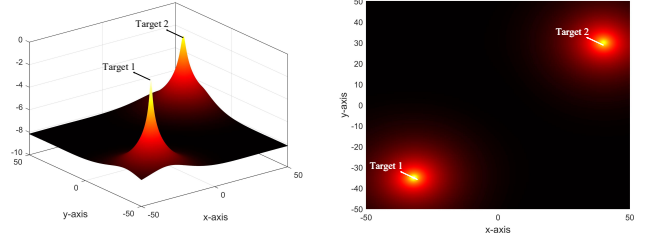
$$\begin{aligned} \Omega_{p,p} &= \frac{2}{\sigma_n^2} \text{Re} \left\{ \left(\frac{\partial s_{p,l}}{\partial \psi_{p,l}^g} \right)^* \left(\frac{\partial s_{p,l}}{\partial \psi_{p,l}^g} \right) \right\} \\ &= \frac{2}{\sigma_n^2} \sum_{m,k,n} |\beta_{p,l}|^2 (2\pi m d / \lambda)^2 \\ &= \frac{4\pi^2 |\beta_{p,l}|^2 d^2 M (M+1) (2M+1) K N}{3\sigma_n^2 \lambda^2}, \end{aligned} \quad (28)$$

$$\begin{aligned} \Upsilon_{p,p} &= \frac{2}{\sigma_n^2} \text{Re} \left\{ \left(\frac{\partial s_{p,l}}{\partial \tau_{p,l}} \right)^* \left(\frac{\partial s_{p,l}}{\partial \psi_{p,l}^g} \right) \right\} \\ &= \frac{2}{\sigma_n^2} \sum_{m,k,n} |\beta_{p,l}|^2 (-2\pi n \Delta f) 2\pi m d / \lambda \\ &= \frac{-2\pi^2 |\beta_{p,l}|^2 \Delta f d M (M+1) N (N+1) K}{\sigma_n^2 \lambda}. \end{aligned} \quad (29)$$

To derive the CRLB, we need to establish the relationship between $\mathbf{\Xi}_l$ and the target position $\mathbf{p}_l^t = [x_l^t, y_l^t]^T$ using the Jacobian matrix. The geometric relationships are given as follows:

$$\tau_{p,l} = \frac{2 \|\mathbf{p}_p^a - \mathbf{p}_l^t\|}{c}, \quad (30)$$

$$\tan(\theta_{p,l}^g) = \frac{y_l^t - y_p^a}{x_l^t - x_p^a}. \quad (31)$$



(a) 3D plot

(b) Top view

Fig. 3: Cost function of the proposed algorithm.

where $\theta_{p,l}^g$ is the AoA in the global coordinate. Thus, the Jacobian matrix is expressed as

$$\mathbf{\Theta} = \frac{\partial \mathbf{\Xi}_l}{\partial \mathbf{p}_l^t} = \begin{bmatrix} \frac{\partial \tau_{1,l}}{\partial x_l^t} & \dots & \frac{\partial \tau_{P,l}}{\partial x_l^t} & \frac{\partial \psi_{1,l}^g}{\partial x_l^t} & \dots & \frac{\partial \psi_{P,l}^g}{\partial x_l^t} \\ \frac{\partial \tau_{1,l}}{\partial y_l^t} & \dots & \frac{\partial \tau_{P,l}}{\partial y_l^t} & \frac{\partial \psi_{1,l}^g}{\partial y_l^t} & \dots & \frac{\partial \psi_{P,l}^g}{\partial y_l^t} \end{bmatrix}, \quad (32)$$

where the elements of the Jacobian matrix can be calculated as follows

$$\frac{\partial \tau_{p,l}}{\partial x_l^t} = \frac{2(x_l^t - x_p^a)}{c \sqrt{(x_l^t - x_p^a)^2 + (y_l^t - y_p^a)^2}}, \quad (33)$$

$$\frac{\partial \tau_{p,l}}{\partial y_l^t} = \frac{2(y_l^t - y_p^a)}{c \sqrt{(x_l^t - x_p^a)^2 + (y_l^t - y_p^a)^2}}, \quad (34)$$

$$\frac{\partial \psi_{p,l}^g}{\partial x_l^t} = \frac{(y_l^t - y_p^a)^2}{\left(\sqrt{(x_l^t - x_p^a)^2 + (y_l^t - y_p^a)^2} \right)^3}, \quad (35)$$

$$\frac{\partial \psi_{p,l}^g}{\partial y_l^t} = -\frac{(x_l^t - x_p^a)(y_l^t - y_p^a)}{\left(\sqrt{(x_l^t - x_p^a)^2 + (y_l^t - y_p^a)^2} \right)^3}. \quad (36)$$

Finally, the CRLB for estimating the target position \mathbf{p}_l^t is given by

$$\text{CRLB}(\mathbf{\Xi}_l) = (\mathbf{\Theta} \mathbf{F} \mathbf{\Theta}^T)^{-1}. \quad (37)$$

V. SIMULATION RESULTS

Unless noted otherwise, the simulation parameters are set as follows: the system consists of five BSs uniformly distributed along a circle with a 500 m radius. They are equipped with an 8-antenna ULA pointing towards the center of the circle. The system uses a carrier frequency of 4.9 GHz and a subcarrier spacing of $\Delta f = 30$ kHz. A sensing task is executed over $N = 7$ OFDM symbols and 8 Resource blocks (RBs). According to the standard in [10], each RB contains 12 subcarriers and the total period of OFDM symbol (including the cyclic prefix) is $35.677 \mu\text{s}$. The beamforming vectors are randomly selected from the complex unit circle to ensure the generation of an approximately omnidirectional beam [3] [7]. Two targets with an radar cross-section (RCS) of 0.01 m^2 are located at $[-32, -35]$ m and $[40, 30]$ m, respectively. The path loss is calculated by the following model [11]:

$$\text{PL} = 103.4 + 20 \lg f_c + 40 \lg d - 10 \lg \sigma, \quad (38)$$

where d is the distance in km from the target to the AP and f_c is the carrier frequency in MHz and σ is the RCS in m^2 . The simulation results are averaged over 1,000 independent Monte Carlo trials. The sensing performance is evaluated using the root mean square error (RMSE) metric, i.e.,

$$\text{RMSE}(\mathbf{p}^t) = \sqrt{\frac{1}{L} \sum_{l=1}^L \|\hat{\mathbf{p}}_l^t - \mathbf{p}_l^t\|^2}. \quad (39)$$

To evaluate the proposed cooperative sensing algorithm, we further compare it with three baselines, defined as follows:

- **Benchmark 1:** As proposed in [5], APs first utilize the spatial smoothing-based tensor decomposition to estimate the parameters of the targets. Then, data association and fusion sensing are achieved by solving the minimum spanning tree algorithm and a nonlinear optimization problem.
- **Benchmark 2:** Inspired by [6], APs utilize only the time delay information for sensing instead of constructing EVA, while its fusion framework follows the subspace-based approach.
- **Benchmark 3:** As proposed in [8], APs implements a Bayesian probabilistic fusion algorithm by constructing a constrained maximum a posteriori (MAP) problem.

Fig. 3a and Fig. 3b intuitively demonstrate that the cost function yields two distinct peaks precisely at the true target locations. The step-by-step procedure for searching these spectral peaks is outlined in Algorithm 1.

As shown in Fig. 4a, the proposed algorithm achieves the best performance. The localization error of the proposed algorithm is significantly lower than that of the existing benchmarks and closely approaches the square root of the CRLB (Root CRLB). This superiority stems from the algorithm's ability to fully exploit the cooperative gain among APs by constructing the EVA array and subspace fusion. In contrast, the data association in Benchmark 1 relies on the parameter extraction results from tensor decomposition of the single AP, which leads to severe performance degradation when parameter extraction fails. The performance of Benchmark 2 not only validates the feasibility of the subspace fusion method but also confirms that constructing the EVA array effectively improves sensing accuracy. Benchmark 3 is restricted by its inherent error floor because the Bayesian probability-based fusion method exhibits limited performance in multi-target scenarios.

Fig. 4b shows the Root CRLB and estimated RMSE versus the number of targets, where the SNR is set to 5 dB. It is evident that the proposed algorithm exhibits superior scalability, maintaining a much lower RMSE compared to other benchmarks. Specifically, the scalability of Benchmark 1 is limited by the fragility of its single-AP processing, which results in frequent association mismatches as the number of targets increases. Alternatively, Benchmark 3 suffers from severe resolution loss. The proposed algorithm mitigates this drawback via subspace fusion. The performance of Benchmark 2 is limited by the number of subcarriers. The proposed algorithm mitigates this drawback via constructing the EVA array to expand the sensing aperture.

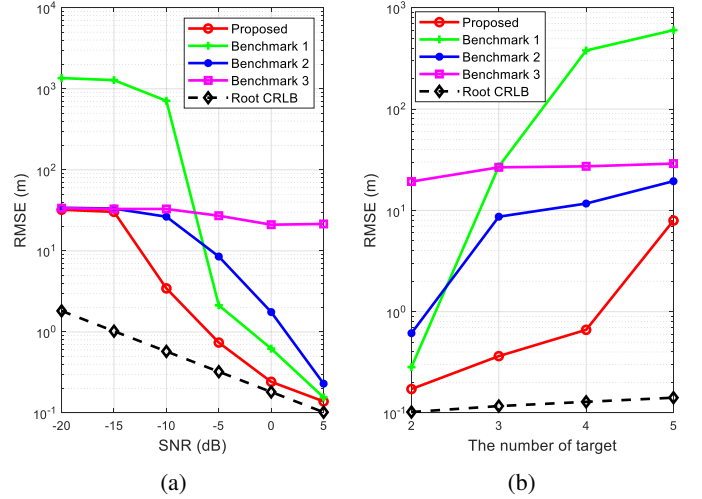


Fig. 4: Square root of the CRLB and estimated RMSE as a function of (a) the SNR and (b) number of targets.

VI. CONCLUSION

In this paper, we proposed a novel data association-free subspace fusion algorithm for cooperative ISAC systems. We constructed an EVA array to expand the sensing aperture via tensor unfolding, which effectively bypasses the complex data association procedures. Furthermore, a derivation of the CRLB was presented. Simulation results demonstrated that the proposed algorithm achieved the best sensing performance compared with existing techniques and closely approached the Root CRLB.

REFERENCES

- [1] F. Liu *et al.*, "Integrated sensing and communications: Toward dual-functional wireless networks for 6G and beyond," *IEEE J. Sel. Areas Commun.*, vol. 40, no. 6, pp. 1728–1767, Oct. 2022.
- [2] Y. Jia, Y. Sun, R. Mao, Z. Nan, S. Zhou, and Z. Niu, "C-mass: Combinatorial mobility-aware sensor scheduling for collaborative perception with second-order topology approximation," *IEEE Trans. Veh. Technol.*, pp. 1–17, 2025.
- [3] R. Zhang *et al.*, "Integrated sensing and communication with massive MIMO: A unified tensor approach for channel and target parameter estimation," *IEEE Trans. Wireless Commun.*, vol. 23, no. 8, pp. 8571–8587, Aug. 2024.
- [4] Y. Zhang, R. Li, C. Pan, H. Ren, T. Wu, and C. Wang, "Modular XL-array-enabled 3-D localization based on hybrid spherical-planar wave model in terahertz systems," *arXiv preprint arXiv:2504.13455*, 2025.
- [5] J. Tang *et al.*, "Cooperative ISAC-empowered low-altitude economy," *IEEE Trans. Wireless Commun.*, vol. 24, no. 5, pp. 3837–3853, May 2025.
- [6] Z. Zhang *et al.*, "Target localization in cooperative isac systems: A scheme based on 5G NR OFDM signals," *IEEE Trans. Commun.*, vol. 73, no. 5, pp. 3562 – 3578, May 2025.
- [7] H. Liu *et al.*, "Multipath component-aided signal processing for integrated sensing and communication systems," in *Proc. IEEE Wireless Commun. Netw. Conf. (WCNC)*, 2025, pp. 1–7.
- [8] S. Liu *et al.*, "Bayesian probability fusion for multi-ap collaborative sensing in mobile networks," *arXiv:2512.02462*, 2025.
- [9] P. E. Gill and W. Murray, "Quasi-newton methods for unconstrained optimization," *IMA J. Appl. Math.*, vol. 9, no. 1, pp. 91–108, Apr. 1972.
- [10] 3GPP, "5G; NR; user equipment (UE) radio transmission and reception; part 1: Range 1 stand alone," 3rd Generation Partnership Project (3GPP), Technical Specification (TS) 38.101-1, Jul. 2023, version 17.10.0. [Online]. Available: https://www.etsi.org/deliver/etsi_ts/138100_138199/13810101/.
- [11] ITU, "Calculation of free-space attenuation," International Telecommunication Union (ITU), Recommendation (R) P.525-4, Aug. 2019. [Online]. Available: <https://www.itu.int/rec/R-REC-P.525>.